AIP | Review of Scientific Instruments

Heating system of pellet samples integrated with terahertz spectrometer

L. A. Sterczewski, M. P. Grzelczak, and E. F. Plinski

Citation: Review of Scientific Instruments **87**, 013106 (2016); doi: 10.1063/1.4939755
View online: http://dx.doi.org/10.1063/1.4939755
View Table of Contents: http://scitation.aip.org/content/aip/journal/rsi/87/1?ver=pdfcov
Published by the AIP Publishing

REVIEW OF SCIENTIFIC INSTRUMENTS **87**, 013106 (2016)

Heating system of pellet samples integrated with terahertz spectrometer

L. A. Sterczewski,[a] M. P. Grzelczak, and E. F. Plinski
Department of Electronics, Wroclaw University of Technology, 27 Wybrzeze Wyspianskiego St., 50-370 Wroclaw, Poland

(Received 15 June 2015; accepted 28 December 2015; published online 19 January 2016)

This article describes automation of temperature-dependent terahertz spectroscopic experiments. The proposed dual-heater temperature controller based on a cascade proportional-integral-derivative algorithm provides smooth temperature changes in the polyethylene-based pharmaceutical pellet samples. The device has been integrated with a terahertz time-domain spectrometer. Thermodynamic experiments can now be performed without any probe inserted into the measured sample. Selected results of temperature-induced evolution in terahertz spectra are presented. © *2016 AIP Publishing LLC.* [http://dx.doi.org/10.1063/1.4939755]

I. INTRODUCTION

Solid samples for spectroscopic experiments are usually prepared by mixing the chemical compound to be investigated with an optically transparent powder and then compressing it under pressure into a pellet. Pharmaceutical pellet samples are popular in spectroscopic studies[1,2] as they are easy to produce. In absorption spectroscopy, the measured spectrum of the sample is compared with the spectrum of the reference — a sample of pure diluting agent. This is done to cancel out instrumental properties and the response of the diluent itself. Over the last decade, this form of sample has been widely used in studies of many solid-state pharmaceuticals carried out using the terahertz time-domain technique.[3]

Selected substances exhibit a (pseudo)polymorphism, which is a phenomenon where a substance can exist in more than one possible crystal structure. Since it changes the physical properties of a drug, such as stability and solubility, it plays a very important role in the pharmaceutical industry. Unwanted polymorphic transitions affect the efficiency of medicines and the shelf life of the final product. Recent research shows that 85% of the active pharmaceutical ingredients (API) have polymorphic forms.[4] Todays' drug development process pushes scientists to investigate the possible polymorphs and their transition conditions, in order to select the most thermodynamically stable form.

Polymorphism detection can, *inter alia*, be accomplished with the use of the terahertz time-domain spectroscopy (THz-TDS).[5] Terahertz waves, which serve to fill the gap between the microwaves and infrared radiation, have been the subject of intense research over the past two decades, due to their unique features.[6] Large organic molecules in crystalline form exhibit terahertz resonances which allow them to be distinguished by the THz-TDS technique[7,8] within the frequency range of 0.1-10 THz.

The acquisition time of the terahertz spectrum is fast enough (from seconds down to milliseconds) to allow for continuous monitoring of a substance. The aforementioned necessity of studies of polymorphic transitions (caused for instance by temperature)[9] has created a demand for a fully automated system for the heating of pharmaceutical pellets in the terahertz regime. It is to be synchronized with a THz-TDS spectrometer.

A. Sample heating problem

Sample heating is a common challenge in many physical and chemical experiments. When the probing radiation (e.g., infrared and X-ray) passes through the investigated object, it may be disturbed by a temperature probe in the beam path. Various heating schemes have been proposed to overcome this difficulty. For instance, the patented solutions for heating of the chemical samples (pharmaceuticals) include a light bulb stored in a receptacle with a thermostat as a controller.[10] Such a construction provides nearly isothermal conditions for the sample with a long-term temperature stability, eliminating the necessity of putting the probe into the sample. However, a large thermal mass of such a chamber makes impossible the use of the fast temperature scanning mode, desired in spectroscopic experiments.

An alternative approach includes a dedicated device for investigating different chemical and physical forms of materials,[11] where a crystalline solid is kept in a computer-controlled heating block. A similar concept of a metal block is employed in a commercially available single-pellet heating chamber,[12] being sufficient to maintain the constant sample temperature. Nonetheless, in both solutions, the center pellet temperature remains unknown and may be significantly different from the contact surface temperature. To eliminate the above issue, a contactless method of sample heating, based on infrared, can be used.[13,14] The radiant energy source uses the projector lamps in order to control the sample temperature in quartz enclosure. Unfortunately, the problem of combining the terahertz pulse with the heat-delivering infrared radiation at normal incidence arises.

In our experiments, we introduced a dual-heater block with two heaters and two pellets: the pellet to be measured and a reference pellet with a temperature probe embedded in the pellet center, thus favoring the contact surface heating method. Measurements have confirmed that the center temperatures of both pellets were nearly identical when supplied from the

[a]lukasz.sterczewski@pwr.edu.pl

same power source owing to the heating block symmetry. In such way, we overcame the problem of the contact surface — pellet center temperature offset. After all, temperature control of the multi-sensor heating system, providing fast response to the set-point change, lack of overshoots, and high temperature stability, was to be designed.

Before the system was developed, we used a separate dual-heater hysteresis controller. It introduced unwanted oscillations in the temperature of the pellets and did not collect information on the temperature at the center of the reference pellet. Furthermore, manual setting of the temperature, without any synchronization with the spectrometer, had in the past been a source of time-related errors. This made the thermodynamic studies in our previous experiments unreliable. As a solution, a microcontroller-based supervisory control and data acquisition (SCADA) device was thus designed and assembled. The supervisory application was developed using LabVIEW's graphical programming environment, widely used in the automation of laboratory experiments.[15,16] In recent decades, LabVIEW has come to be applied in spectroscopic[17] and photonic instrumentation.[18]

Thermodynamic experiments performed with the equipment can be divided into two groups. (1) Temperature scanning with a predefined rise-profile, used for substance stability tests and for comparison with the results of differential scanning calorimetry (DSC). (2) Maintaining of a constant temperature over time for studying the kinetics of a reaction. Clearly, long-term temperature stability and excellent set-point tracking performance were the main requirements. In this article, we present a dual-heater temperature controller with a cascade proportional-integral-derivative (PID) algorithm, operating under the supervision of a LabVIEW-based SCADA application.

II. SPECTROMETER EQUIPMENT

The pharmaceuticals were examined with a home-built terahertz time-domain spectrometer. A simplified diagram of the system is shown in Fig. 1. The low-temperature-grown GaAs photoconductive antennas (Tx and Rx) are pumped by femtosecond optical pulses, generating terahertz radiation between 0.1 and 3 THz.[19] The dual-heater block is placed at the focal point of the two off-axis parabolic mirrors guiding the THz radiation. The generated pulse passes through the investigated sample, without being interrupted by any obstacles, e.g., temperature sensors. In contrast, in the scheme with a symmetrically placed reference pellet, their presence affects the measurement.

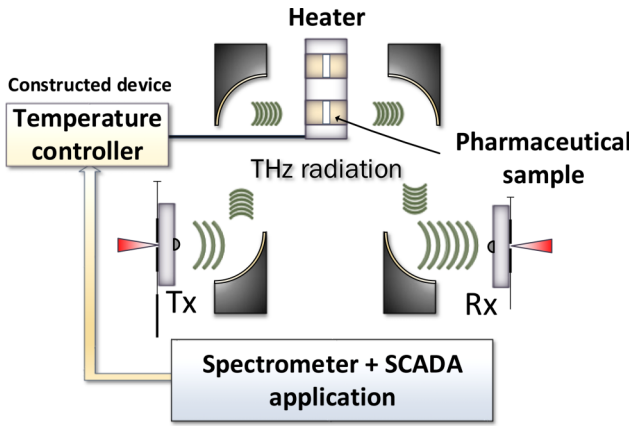

FIG. 1. Simplified diagram of the measurement system.

To detect the pulse, a coherent homodyne detection scheme with a lock-in amplifier was used (SRS830). The transmitting antenna is biased by an alternating square-wave of the kHz-frequency range signal. The receiving antenna converts the terahertz electric field into photo-current. The terahertz pulses can be reconstructed by means of a time-shift of the femtosecond laser pulses performed by the motorized delay line.

The dual-pellet heater is made of an aluminum block with brass-coated AC electric heaters. They are equipped with built-in temperature sensing J-type thermocouples. The internal diameter of the heating chambers is equal to 13 mm, the size of sample broadly used in spectroscopic studies. The temperature inside the reference pellet is measured by the special K-type thermocouple. To ensure a reliable thermal contact, a small hole was drilled in the central part of pellet and filled with the thermal grease when assembling the temperature probe. Should the tolerance of the thermocouple prove to be unsatisfactory, a dedicated interface for PT100 platinum resistance sensors can be used as an alternative.

To allow for optimum supervision of the heating process, we introduced an autonomous and maintenance-free item of apparatus — the heater controller. We focused our attention on the cascade temperature control algorithm because it delivers a reasonably short rise-time, significantly reducing the temperature overshoots inside the pellets during setting of the transient. This required support for multiple temperature sensors, so we added a few analog interfaces with possibility of expanding them further. The PC control software was developed in the LabVIEW environment. The existing virtual instrument spectrometer, because of the software model selected, could be readily integrated with the heater controller software. The user interface window of the application is shown in Fig. 2.

III. MODELING

Thermal objects are a rewarding class of computer experiments with a well-developed systems theory and a practical background of use in the food or chemical industry, for instance. Implementation and tuning of the robust and no-overshoot control algorithm are both a challenging and time-consuming task. The bases of the mathematical models can be constructed based on the physical parameters of the object. The objective of such a procedure is to omit real-object experiments, due to the significant time intervals between the subsequent step response tests, as well as potentially destructive thermal effects.

A. Mathematical model

The formula for transfer of the thermal energy Q in terms of temperature change ΔT is given by

$$Q = C_{th}\Delta T \text{ (J)}, \quad (1)$$

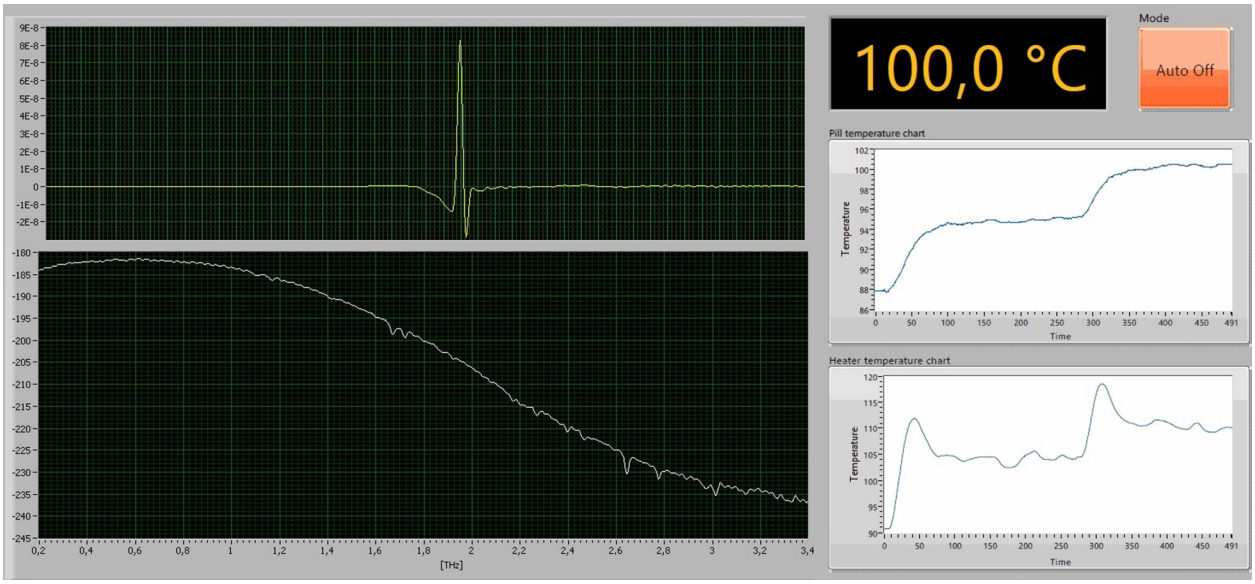

FIG. 2. The application software for the experiment. The left side shows the spectroscopic measurements (a pure nitrogen transmission impulse and its spectrum are shown here). The right side shows a panel for the temperature control process.

where C_{th} denotes the thermal mass (heat capacity) of the object. This term is also known as the thermal flywheel.[20] It provides resistance against temperature fluctuations. The larger the thermal mass, the more significant the delay is that is present in a step response at constant power. The thermal mass of a uniformly composed body is a product of its mass and specific heat c_p, denoted as

$$C_{th} = mc_p = \rho V c_p. \tag{2}$$

Heat transfer rate $dQ(t)/dt$ — can be expressed as a sum of heat sources and heat losses — $q_i(t)$,

$$\frac{dQ(t)}{dt} = C_{th}\frac{dT(t)}{dt} = \sum q_i(t)\ (\text{W}). \tag{3}$$

Using the Newton's law of cooling, the heat loss ($q_{\text{loss}} = q_i$) can be expressed as

$$q_{loss}(t) = -K\Delta T(t) = -hA[T(t) - T_{Amb}]\ (\text{W}), \tag{4}$$

where K is a thermal proportionality constant, equivalent to a product of the heat transfer coefficient h and heat transfer surface area A. In the above formula, T_{Amb} is the ambient temperature and $\Delta T(t)$ denotes the time-dependent thermal gradient. When the body is hotter than environment, the gradient $\Delta T(t)$ is positive (it is cooling down). Thus, the minus sign in the formula indicates that the heat power is transferred from the system to the ambient environment.

Finally, when a single heat source (q_{H}) and a single heat loss (q_{loss}) are present, the heat transfer rate is expressed as

$$\frac{dQ(t)}{dt} = q_{\text{H}}(t) + q_{\text{loss}}(t) = \\ = q_{\text{H}}(t) - hA[T(t) - T_{Amb}]\ (\text{W}). \tag{5}$$

The above equation can be rewritten in the terms of thermal mass C_{th}, the thermal proportional coefficient K, and temperature change $dT(t)/dt$,

$$C_{th}\dot{T} = C_{th}\frac{dT(t)}{dt} = q_{\text{H}}(t) + q_{\text{loss}}(t) = \\ = q_{\text{H}}(t) - K[T(t) - T_{Amb}]. \tag{6}$$

Dividing the equation by C_{th}, we obtain the final form of the heat transfer equations,

$$\dot{T}(t) = \frac{dT(t)}{dt} = \frac{1}{C_{th}}\left[q_{\text{H}}(t) - K(T(t) - T_{Amb})\right]. \tag{7}$$

A set of heat transfer equations in the form shown above was used to model the heating system under consideration.

B. Transfer function

In practice, when a short-time model is desired, the state-space model can be replaced by a more convenient, but less accurate transfer function model. Within the described device, it proved to be less difficult to implement. The equations presented here however provide the basis for its derivation. For the sake of simplicity, we considered in our model a single heating block (Fig. 3), as the second block is identical.

Assuming slow changes in ambient temperature T_{Amb}, the differential equations can be resolved into two multiplicative transfer functions. Such a representation separates the power change response of the heater from the change in pellet temperature, giving independent terms.[21] This is done by introducing two effective time constants in the denominator of the transfer function, which reflect the parameters K_i and C_i of the materials.

The first transfer function, describing the heater response, implements Küpfmüller's 1st order model with a transport delay of 5 s.

$$G_{Q\to H} = e^{-5s} \cdot \frac{280}{65s + 1}\ . \tag{8}$$

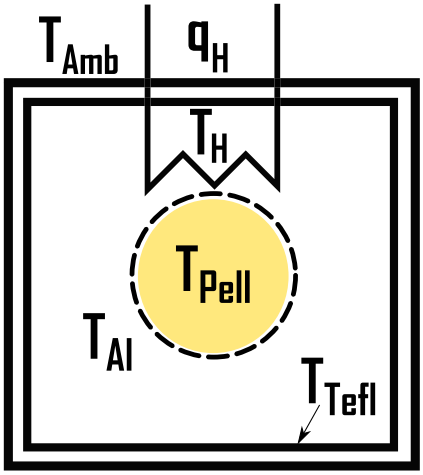

FIG. 3. Simplified single-heater model. The assumed state temperatures are defined as temperature of the heater T_H, of the Teflon coating T_{Tefl}, aluminum body T_{Al}, pellet T_{Pell}, ambient temperature T_{Amb}, and a heat power source q_H, respectively.

The second transfer function, representing the influence of heater's temperature on the pellet, is given by

$$G_{H\to P} = \frac{277/280}{85s+1}\,. \tag{9}$$

The resulting transfer function, with the heater power input and the pellet temperature output, is a product of the two components above,

$$G_{Q\to P} = G_{Q\to H}\cdot G_{H\to P} = \frac{e^{-5s}\cdot 277}{(65s+1)(85s+1)}\,. \tag{10}$$

By definition, the transfer function includes the zero-valued initial conditions. To start the simulation with an initial value equal to the room temperature, it has to be added in the output summation block.

C. Matlab simulation

The transfer function model was implemented in the Simulink (MathWorks) environment. The results of the simulation, carried out for the 44-s square pulse response (100% duty cycle of heater power delivered), compared with real data, are shown in Fig. 4.

The model fits with the experimental data with a good level of match. Simulation of the single-heater system with the various types of controlling algorithms (single PID, MBC, cascade PID) led to a significant reduction in overshoot, while preserving as high a rise-time as possible.

IV. CONTROL ALGORITHM

The performance of the pellet heating system is determined by a non-trivial cascade PID control algorithm. On the first attempt, a classical independent PID structure was tested. Major disadvantages involving large overshoots in the pellet's temperature, and gathering information only from one sensor used in the control process, excluded this approach from being used for the type of precise measurements that we conduct.

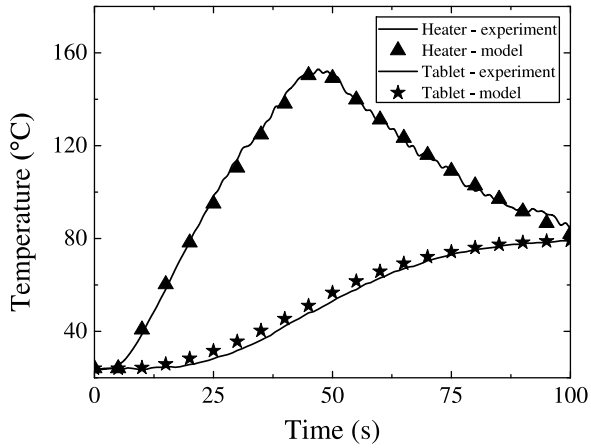

FIG. 4. Square pulse response of the heater and pellet.

Accurate control of large thermal lag systems can be accomplished with a modified version of the basic PID — a dual-feedback cascade PID controller. The block diagram of this control algorithm is shown in Fig. 5. With this approach, information concerning both the local (heater) and the global (pellet) temperature are used in the control process. The main feature of this scheme is its hierarchical design. The outer supervisory loop provides a set-point that evolves over time for the inner slave loop.

As the thermal lag of the heater is much less than that of the pellet, and the temperature of the heater can fluctuate at a higher frequency, the heater control loop was chosen to be the inner one. It maintains the heater's temperature locally. Also, local feedback allows faster correction of the control error in comparison with the global feedback scheme. It is preferable for objects with a lower time constant to be in the inner control block. Experiments have shown that the inner loop controller can be a simple proportional one, whereas the master must provide an integral action. A cascade algorithm requires the presence of integral action. Otherwise, undamped oscillations in the settling of temperature appear. Though near zero, steady-state error cannot be attained.

In our implementation, we used the PID-IND controller structure with independent proportional, integral, and derivative terms[22] in the supervisory loop. However, the inner loop's derivative and integral terms were disabled, because the integration of the outer loop was sufficient. Furthermore, they did not perform well in the noisy environment.

The polyethylene-based pellet melts down above 120 °C. To prevent this temperature being exceeded and avoid large overshoots, specific non-linear blocks had to be introduced. The cutoff limit for the heater's temperature was set to 115 °C. Above this threshold, power is disabled. Then, a saturation block was introduced. It makes negative control impossible, as there is no cooling feature of the heater and limits the heater's power to 16% of its nominal 250 W. The next non-linear block, introduced into the master PID controller, is an integral windup cancellation. It freezes the integral block when full heater power is delivered. Only when the heater is supplied and the process value (pellet's current temperature) is below the set-point, the integral block is allowed to operate. When in an overshoot state, the integral block is initialized with

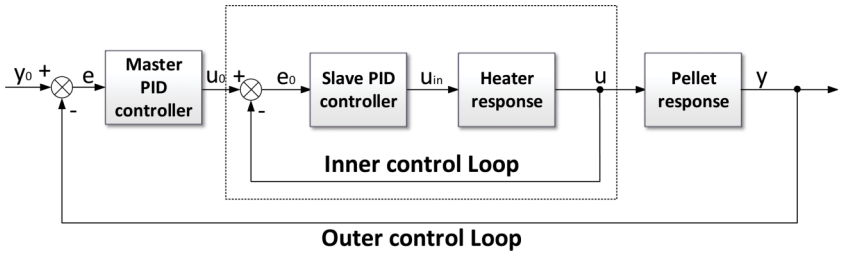

FIG. 5. Cascade PID control algorithm.

the current process value. It is crucial to initialize it in the start-up routine with the prescaled value of heater's current temperature (prescaled by the integrator's gain). Otherwise, it takes a very long time for the integrator to accumulate the error. The startup lag of this block can make overshoot-free control of the main loop impossible. In addition, saturation of the integral block (both positive and negative) was introduced to minimize the risk of large integral block windup. The discrete PID control time interval was set to 330 ms. This interval was sufficiently frequent to control the object with a thermal type of response.

In the cascade control scheme, it is preferable for the inner loops to be tuned first. The proportional term in the inner loop was found to provide the fastest and non-oscillative character for $K_p = 3.4$. The outer loop's proportional and integral term were set to $K_p = 1.3$ and $K_i = 0.04$, respectively, where K_i is the equivalent of the ratio K_p/T_i in the PID-ISA (Ideal Standard Algorithm). High proportional gain in the inner loop ensures rapid error correction, whereas the lower gain in the master loop results in smoother transitions.

When no liquid nitrogen source is available to cool down the experiment, tuning of systems with large thermal lag controlled by the cascade PID can be demanding and time-consuming. In practice, intervals between subsequent experiments with new controller gain settings can exceed several tens of minutes. Our work showed that the controller's structure and the coarse values of their gain coefficients can be derived by numerical simulations, reducing the number of possible step excitation experiments to obtain the desired response. The object with the hierarchical controller structure was simulated in the *Simulink* environment. Slight corrections (±20%) of the inner loop proportional term gain, and the outer integral term gain, in the real-life system were verified experimentally. A fine-tuning procedure, based on the parameters proposed from the simulation, ensured the best possible controller gain settings within the proposed region of values.

As the two heating chambers are almost identical, the concept of two cascade control systems running in parallel with their own heater temperatures and a shared pellet temperature gave satisfactory results. It was sufficient to keep the heater temperatures equal to an accuracy of within (±0.5 °C) and keep the difference in pellet temperature (between the reference and measured temperature) even lower.

V. RESULTS

The step change in the measured pellet's temperature set-point from 87 °C to 94 °C is shown in Figs. 6(a) and 6(b). The rapid increase in the temperature at the center of the pellet is achieved by introducing a small overshoot in the settling of the heater's temperature. Without this, the rise-time of the pellet would be unsatisfactorily long. It would disable the set-point tracking control mode, as the offset between the set-point varying over time and the actual temperature of the pellet would be too high.

Due to favorable behavior of the system in terms of dynamics, we accepted some tunings of the PID controller parameters. Although, after the first overshoot, only minimal fluctuations appear, their influence on central temperature of the pellet is minimal, and the aforementioned temperature spike only minimizes the rise-time of the pellet's temperature.

The tuned system was used to study the dehydration of a well-known polycrystalline hydrate — the α-D-glucose monohydrate — in the terahertz regime. The compressed 400 mg pellet sample with 10% of glucose was placed in the heating chamber. The 360 mg polyethylene pellet was used in the neighboring chamber as a temperature reference. The terahertz path was enclosed in an acrylic box filled with pure nitrogen for the elimination of water vapor. We performed an 80-min dehydration experiment at a heating rate of 1 °C/min in the temperature scanning mode. The performance of the system

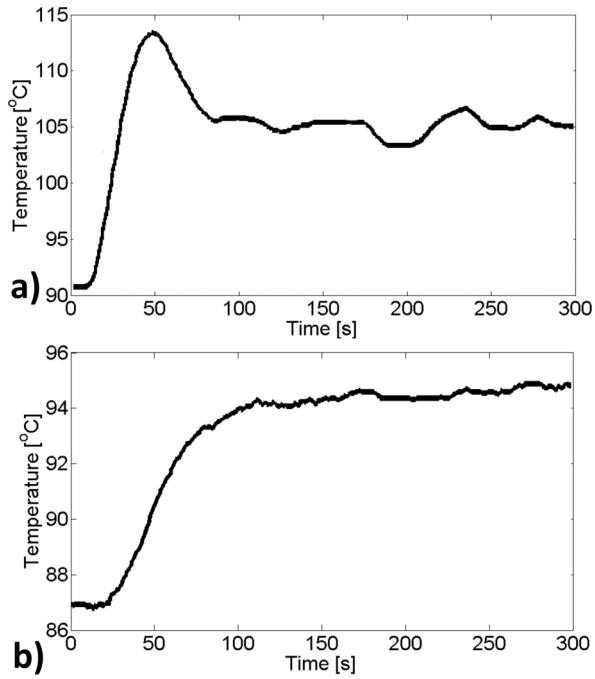

FIG. 6. Step change of pellet's temperature set-point from 87 °C to 94 °C. (a) Step response of the heater. (b) Step response of the pellet.

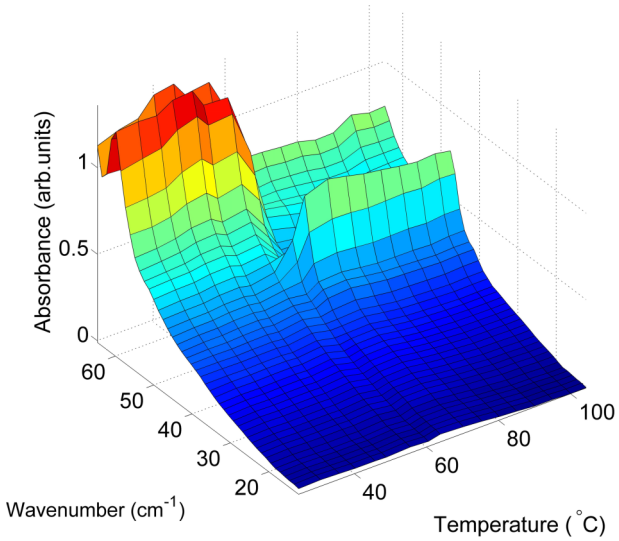

FIG. 7. Glucose dehydration process in THz light. The kinetics of the transition were studied in details.[12]

was sufficient to maintain required rate. The evolution of the spectrum is shown in Fig. 7. The dehydration moment is clearly visible, thus a detailed analysis of the decomposition rate can be performed in that particular temperature range.

The dehydration process examined with our method enabled the detection of the phase transition moment at approximately 65 °C. This result has been confirmed by the DSC analysis,[23] where the peak of the thermograms in the dehydration process appeared at around 70-75 °C, depending on the preparation of the samples. This slight discrepancy may be caused by significantly different experimental conditions in the DSC-monitored dehydration experiment, where the relative humidity throughout the experiment exceeded 0%, whereas we kept the sample in a dry nitrogen atmosphere, as the THz spectroscopic method is exceedingly sensitive to water vapor. Additionally, the heating rate ($\Delta T/\Delta t$) and construction of the DSC sample pan are known to contribute to varying results — in the aforementioned studies, the pan was covered with a non-hermetic lid, thus changing the dehydration environment compared to our experiment.

The presented investigation technique can be considered as supplementary to the DSC, since recent research on phase transition detection in the industry shows, that two or more simultaneous methods should be employed to monitor the process reliably.[24] Our studies on thermodynamics of derivatives of a non-steroidal anti-inflammatory drug — Piroxicam[25] have shown that one may not detect the same phase transitions with THz spectroscopy, as using the DSC technique. Consequently, the thermo-analytical methods should be accompanied by spectroscopy to minimize the risk of overlooking changes in the examined samples.

In addition to the temperature-scanning experiments, the constant-temperature (isothermal) ones were also enabled by our system. They allow to study the phase transition kinetics. We prepared the α-D-lactose monohydrate sample (in the same manner as in the temperature scanning experiment) and heated it for 90 min at 100 °C, wherein the sample underwent a pseudo-polymorphic phase transition — the dehydration.

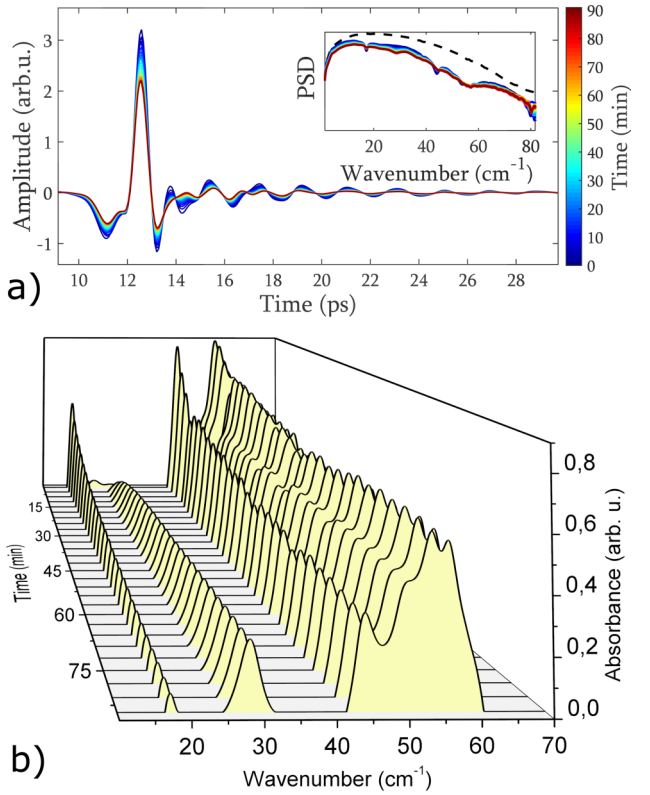

FIG. 8. Demonstration of the constant temperature (isothermal) mode: α-D-lactose monohydrate dehydration process in THz light. The monohydrate was kept at 100 °C for 90 min. (a) Evolution of the time-domain signal and the power spectral density; dashed line marks the reference signal. (b) The absorption spectrum with removed baseline; the spectral area of the absorption peaks evolving in the 15–35 cm^{-1} band was used for quantitative analysis.

Figs. 8(a) and 8(b) show the evolution of the time-domain signal and absorption spectra of lactose with removed baseline, respectively. The pre-processed spectra were used to perform the quantitative analysis — estimate the normalized dehydration fraction α in time. We integrated the peak area (PA) between 16 and 19 cm^{-1}, corresponding to the first peak, 25 and 32 cm^{-1} of the second peak, and applied the broadband Bayesian spectral sources (BSS) algorithm using the full spectral information.[26] Peaks between 42 and 62 cm^{-1} cannot be used in the peak-area method since there is a significant cross-band between them. It should be noted that in the Bayesian approach, we respect the full additivity constraints, meaning that the sum of the dehydrate and the hydrate fraction at each time instant adds to one.

Fig. 9 shows the evaluation of the dehydration fraction α of α-D-lactose monohydrate as a function of time (inset) and the dehydration rate constant k (main plot) using the three methods. In order to estimate the dehydration rate constant k, the dehydration kinetics model must be carefully selected, mostly from the known rate laws. One needs to find a transformation of α versus time t, such that the transformed points exhibit a linear trend. While in many dehydration experiments, the sigmoidal-like reaction profile is expected, the curve of $\alpha(t)$ in this study exhibits a deceleratory trend — the reaction slows down with time. The best fit (with the highest correlation coefficient r) to the experimental points of α was found with

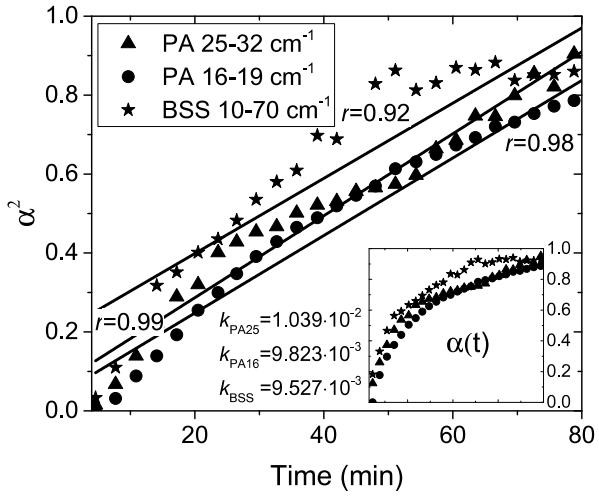

FIG. 9. Plot of the normalized α-D-lactose dehydration fraction α versus time (inset) and evaluation of the dehydration rate k according to the deceleratory one-dimensional diffusion model D1. Straight lines represent the linear fits to the data.

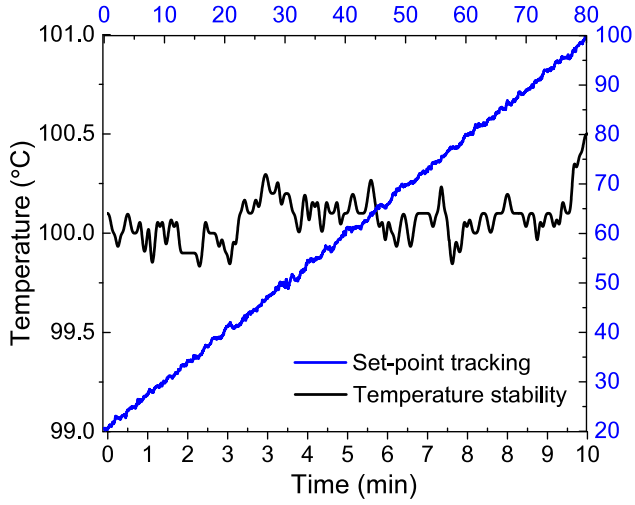

FIG. 10. 10-min temperature stability in the isothermal dehydration experiment (black) and the resulting temperature of the 90-min set-point tracking mode experiment (blue).

the one dimensional diffusion D1 model[27] — a member of the constant deceleratory rate law family of reactions in solids, given by

$$\alpha^2 = k \cdot t\,. \tag{11}$$

The dehydration rate constants k found with three different methods are $1.039{\cdot}10^{-2}$ min^{-1} for the integrated peak between 25 and 32 cm^{-1}, $9.823{\cdot}10^{-3}$ min^{-1} for the integrated peak between 16 and 19 cm^{-1}, and $9.527{\cdot}10^{-3}$ min^{-1} for the broadband Bayesian approach. The corresponding correlation coefficients are $r = 0.99$, $r = 0.98$, and $r = 0.92$, respectively. The relative differences (absolute difference divided by the mean of two compared) between the estimates are within acceptable tolerance — less than 10%. Since it is not obvious which spectral region corresponds best to the physical change, the water loss from the crystal lattice, it is reasonable to calculate the arithmetic mean of the dehydration rates — $9.913{\cdot}10^{-3}$ min^{-1} — or correlation-coefficient weighted mean to favor the best fit — $9.923{\cdot}10^{-3}$ min^{-1}. By repeating the experiment at different temperatures, one can generate the Arrhenius plot, which relates the natural log of k to the reciprocal of the absolute temperature. The plot is used to study the effect of temperature on the rates of the polymorphic transitions in a drug. Owing to the fact that the temperature of the water loss in α-D-lactose is 100 °C and above, the diluting medium must be changed from the spectroscopic grade low density polyethylene (LDPE) to Teflon (PTFE), for instance, to prevent the sample from melting. This might also involve slight corrections in the controller gains, as the thermal conductivity of PTFE is somewhat lower ($\kappa = 0.25$ W m^{-1} K^{-1}) than that of the polyethylene ($\kappa = 0.33$ W m^{-1} K^{-1}).

The temperature stability in the lactose dehydration experiment is shown in Fig. 10 (black line). The mean temperature and the standard deviation are 100.07 °C and 0.124 °C, respectively. The stability can be further improved by replacing the noise-sensitive thermocouples with the temperature-dependent resistors, for instance. The blue line plots the set-point tracking mode in a drug phase transition experiment. Temperature follows the pre-defined rise profile with low offset — the root-mean-square error (RMSE) is equal to 0.1901.

VI. CONCLUSION

We have presented an extension to the spectroscopic system for the evaluation of heat-induced molecule decompositions in the terahertz frequency band. When a recently synthesized drug with unknown physical properties is to be studied for the existence of the polymorphic phase transitions, the use of our system may significantly simplify the procedure. The temperature scanning mode helps to find the transition region initially. If any evolution is present, the constant temperature mode enables the researcher to study the kinetics of the process in that region. The experiments that we conducted with the α-D-glucose monohydrate, and α-D-lactose monohydrate, prove the concept.

We improved the single-heater scheme by introducing the second reference heater with a known temperature of the pellet's center. A detailed mathematical model and intensive numerical simulations provided the bases for precise temperature control of the measured sample. Such an approach was found to eliminate significant heater-pellet temperature offset. The unique cascade control algorithm with embedded nonlinear blocks reduced the overshoots and oscillations to minimum, preserving a sharp rise-profile. For further improvement of the dynamic response, if it is not satisfactory, a fuzzy controller or a predictive control scheme can be employed simply by modifying the existing software.

The design procedures for the multiple sensor heating system presented here can be employed in different fields of the applied sciences. Often, a second reference object can be introduced to model the behavior of the investigated sample placed symmetrically under the same environmental conditions. This

may significantly reduce control errors at the expense of a slight modification to the measurement system.

ACKNOWLEDGMENTS

The authors would like to thank two anonymous reviewers for their comments, and Dr. K. Nowak for his helpful discussions and assistance with software integration. This work was supported in part by an internal university Grant No. S50037/W4K3.

[1]J. Johansson, S. Folestad, M. Josefson, A. Sparén, C. Abrahamsson, S. Andersson-Engels, and S. Svanberg, Appl. Spectrosc. **56**, 725 (2002).
[2]P. Matousek and A. Parker, Appl. Spectrosc. **60**, 1353 (2006).
[3]H. Namkung, J. Kim, H. Chung, and M. A. Arnold, Anal. Chem. **85**, 3674 (2013).
[4]P. H. Karpinski, Chem. Eng. Technol. **29**, 233 (2006).
[5]G. G. Zhang, D. Law, E. A. Schmitt, and Y. Qiu, Adv. Drug Delivery Rev. **56**, 371 (2004).
[6]M. Tonouchi, Nat. Photonics **1**, 97 (2007).
[7]M. J. Fitch and R. Osiander, Johns Hopkins APL Tech. Dig. **25**, 348 (2004).
[8]C. J. Strachan, P. F. Taday, D. A. Newnham, K. C. Gordon, J. A. Zeitler, M. Pepper, and T. Rades, J. Pharm. Sci. **94**, 837 (2005).
[9]J. A. Zeitler, D. A. Newnham, P. F. Taday, C. J. Strachan, M. Pepper, K. C. Gordon, and T. Rades, Thermochim. Acta **436**, 71 (2005).
[10]A. J. Thomas, "Electric heating apparatus for heat-treating pharmaceuticals," U.S. patent 4,273,992 (16 June 1981).
[11]R. Kobylecki, D. Cowell, and V. Stylianopoulos, "Investigating different physical and/or chemical forms of materials," U.S. patent application 11/160,552 (15 November 2005).
[12]H.-B. Liu and X.-C. Zhang, Chem. Phys. Lett. **429**, 229 (2006).
[13]F. Baum, Rev. Sci. Instrum. **30**, 1064 (1959).
[14]T. Kinsel and T. Seidel, J. Appl. Phys. **33**, 767 (1962).
[15]C. Elliott, V. Vijayakumar, W. Zink, and R. Hansen, J. Assoc. Lab. Autom. **12**, 17 (2007).
[16]I. Kirkman and P. Buksh, Rev. Sci. Instrum. **63**, 869 (1992).
[17]R. Aspey, I. McDermid, T. Leblanc, J. Howe, and T. Walsh, Rev. Sci. Instrum. **79**, 094502 (2008).
[18]J. Bok and P. Schauer, Rev. Sci. Instrum. **82**, 113109 (2011).
[19]P. R. Smith, D. H. Auston, and M. C. Nuss, IEEE J. Quantum Electron. **24**, 255 (1988).
[20]B. Haglund and K. Rathmann, Vital Signs Curriculum Materials Project, Center for Environmental Design, University of California, Berkley, CA (1996).
[21]Y. Lee, S. Park, and M. Lee, Ind. Eng. Chem. Res. **37**, 1859 (1998).
[22]R. Salat and M. Awtoniuk, Neural Comput. Appl. **26**, 1 (2014).
[23]M. Mathlouthi, G. Benmessaoud, and B. Rogé, Food Chem. **132**, 1630 (2012).
[24]D. Giron, J. Therm. Anal. Calorim. **64**, 37 (2001).
[25]B. Szczesniak-Siega, B. Fuglewicz, K. Nowak, B. Szlachetko, L. Sterczewski, G. Beziuk, P. Jarzab, W. Malinka, J. Baran, M. Drozd *et al.*, in *Infrared, Millimeter, and Terahertz waves (IRMMW-THz), 2014 39th International Conference on* (IEEE, 2014), pp. 1–2.
[26]L. A. Sterczewski, M. P. Grzelczak, K. Nowak, B. Szlachetko, and E. F. Plinski, Chem. Phys. Lett. **644**, 45 (2016).
[27]J. E. House, *Principles of Chemical Kinetics* (Academic Press, 2007).